



Design, structural analysis, and ROS-based kinematic simulation of a robotic arm for capsicum harvesting in greenhouse environments

 Ayan Paul¹⁺
 Rajendra
Machavaram²

^{1,2}Agricultural and Food Engineering Department, Indian Institute of Technology, Kharagpur, West Bengal, India.

¹Email: ayanpaul2210@kgpian.iitkgp.ac.in

²Email: rajendra@agfe.iitkgp.ac.in



(+ Corresponding author)

ABSTRACT

Article History

Received: 31 October 2025

Revised: 1 December 2025

Accepted: 3 December 2025

Published: 5 December 2025

Keywords

6-DOF robotic arm
Capsicum harvesting
Forward kinematics
ROS 2 simulation
Structural analysis
Workspace evaluation.

This study presents an integrated mechanical design, structural validation, and kinematic simulation framework for a 6-DOF robotic manipulator tailored to precision capsicum harvesting in greenhouse environments. The robot was designed using a lightweight, modular architecture based on a hybrid-material approach: Polylactic Acid Plus (PLA+) structural links, Thermoplastic polyurethane (TPU) gripper fingers, and stainless-steel scissor cutters. The serial-link configuration was optimized for maneuvering within a canopy width and plant height range, with a total manipulator reach of approximately 700 mm and a payload capacity of 200 g. Structural safety was verified via Finite Element Analysis (FEA) using SolidWorks Simulation, considering direction-specific harvesting loads. Maximum von Mises stress occurred in the shoulder joint (Link 2), while the forearm link (Link 5) showed the highest displacement, both remaining within allowable PLA+ limits. All links exhibited high Factors of Safety, with the minimum being 88.58, confirming mechanical integrity under worst-case loading. Kinematic modeling and motion planning were implemented using a URDF-based robotic model within ROS 2 (Humble), RViz2, and MoveIt2. Forward kinematics showed a mean end-effector pose error of 2.3 mm across sampled target positions, validating model accuracy. The manipulator executed a full harvesting cycle in 6 seconds with sequential joint actuation, including base rotation, arm extension, wrist alignment, and gripping. Reachability and 3D workspace analysis confirmed full coverage of the capsicum canopy (0.40 m radius) within a maximum reach of 0.70 m. The results demonstrate a biologically compatible, structurally safe, and kinematically feasible solution for greenhouse fruit harvesting.

Contribution/Originality: This study contributes to the existing literature by integrating crop-specific morphology into robotic arm design for capsicum harvesting. It employs a new estimation methodology using link-wise FEA and ROS 2-based kinematic validation. This study is among the few that have investigated PLA+ structural safety and full canopy reachability.

1. INTRODUCTION

Capsicum (*Capsicum annuum* L.), commonly known as sweet pepper or “Shimla Mirch,” is one of the most economically significant vegetable crops in India, with an annual production exceeding 500 thousand tonnes, primarily concentrated in states such as West Bengal, Karnataka, and Himachal Pradesh [1]. The increasing demand for high-quality produce and off-season cultivation has driven a significant shift toward protected cultivation systems. Greenhouse farming of capsicum has demonstrated yield improvements of 3–5 times over open-field conditions, while also enhancing fruit uniformity and quality. Nutritionally, capsicum is a valuable source of vitamin C (up to 130–190 mg/100g), vitamin A, and antioxidants such as beta-carotene and flavonoids, making it highly desirable in both

domestic and export markets [2]. However, the intensification of capsicum cultivation within controlled environments introduces several operational challenges, particularly in labor availability, harvesting efficiency, and postharvest handling. Given that capsicum fruits are non-climacteric and highly perishable, timely and precise harvesting is critical to preserving market quality and nutritional value. Manual harvesting, which remains the prevailing method, is not only labor-intensive but also susceptible to inconsistency and physical damage due to human error and fatigue. These limitations are further magnified in greenhouse settings, where the dense canopy, clustered fruit formation, and limited row spacing require high maneuverability and precision. In this context, automation through robotic harvesting systems presents a transformative solution. By leveraging advanced perception systems, motion planning algorithms, and specialized end-effectors, robotic platforms can effectively navigate the spatial constraints and mechanical complexities of greenhouse environments. Such systems offer the potential to reduce dependency on seasonal labor, standardize harvesting practices, minimize fruit loss, and enhance overall operational efficiency, thereby reinforcing the economic viability and scalability of protected agriculture.

A typical robotic harvesting system for capsicum comprises several integrated subsystems working in coordination to enable autonomous operation. These include an RGB-D or multispectral vision module for real-time fruit detection and localization, a robotic manipulator responsible for accurate fruit detachment, a specialized end-effector designed to perform non-destructive gripping and precise peduncle cutting, and a mobile platform capable of navigating the narrow and densely vegetated greenhouse rows [3]. Among these, the robotic manipulator serves as the central actuation unit, bridging the perception system with physical interaction [4]. Its ability to convert high-level sensory inputs into precise motion control is critical for reaching and harvesting fruits situated at varying heights, orientations, and depths within the plant canopy, while also adhering to mechanical and safety constraints to prevent crop or structural damage. However, robotic harvesting in greenhouse environments presents several inherent challenges. Capsicum fruits frequently grow in clusters and are often partially or fully occluded by dense foliage, complicating visual detection and reachability. Moreover, the confined inter-row spacing, complex branching geometry, and limited working envelope further restrict manipulator motion. The stems of capsicum are also delicate and flexible, necessitating compliant and careful interaction to avoid bruising or plant injury. These constraints collectively emphasize the requirement for a robotic manipulator with a high number of degrees of freedom (DoF) and enhanced dexterity [5]. A multi-DoF arm, when integrated with a vision-guided control framework, enables adaptive path planning and orientation control to access occluded fruits, align the end-effector precisely with the peduncle, and execute harvesting actions with minimal collision risk. This motivates the design and development of a lightweight, perception-aware, and mechanically agile robotic arm tailored for greenhouse capsicum harvesting applications.

Computer-Aided Design (CAD) serves as a fundamental tool in developing robotic arms for agricultural tasks by enabling precise joint configuration and geometric optimization for environments like greenhouses. Barth et al. [6] outlined structural and software considerations for agricultural robot subsystems using ROS middleware, highlighting its integration challenges and advantages. Barth et al. [6]. Rahul et al. [7] designed a 4-DOF parallel robot arm for automated seedling handling, achieving a 93.3% success rate with a 3.5 s cycle time, incorporating dual-microcontroller firmware, stepper motor actuation, and 3D CAD-based mechanical modeling. Rahul et al. [7]. Van Herck et al. [8] demonstrated how CAD facilitates spatial planning for robotic systems in dense crop environments, emphasizing navigation and collision avoidance. Van Herck et al. [8]. Liming et al. [9] proposed a dual-arm robot using UR10 manipulators, employing standardized mechanical interfaces and ANSYS Workbench simulations to maintain strength and reduce weight to below 170 kg during live-wire operations. Liming et al. [9]. Huanca et al. [10] introduced “MARS-ROBOT,” an 8-DOF manipulator with a 1.0 m linear track, designed using SolidWorks and tested via MATLAB trajectory simulation and CoppeliaSim operability analysis for industrial painting tasks in Lima. Huanca et al. [10]. Paredes et al. [11] developed a pick-and-place and palletizing cell using SolidWorks and MATLAB-based kinematic modeling for SCARA T6 and UR10 robots, achieving task execution times of 1.18 s and

2.32 s, respectively. Paredes et al. [11]. Salazar and Portero [12] incorporated agricultural constraints such as torque and spatial limits into CAD-based 6-DOF robot arm models using Autodesk Inventor, enabling servo and gripper linkage design via iterative prototyping. Salazar and Portero [12]. Li and Li [13] introduced crop-robot co-design approaches, wherein CAD models aligned robot link design with plant canopy structures to improve reachability and perception. Li and Li [13]. Kuruvilla et al. [14] performed a comparative FEM analysis of a 6-DOF cylindrical arm for automated agriculture, evaluating stiffness across carbon fiber, aluminum, and steel variants under terrain slopes up to 60°, identifying cost-efficient, robust structures for precision farming [14].

Finite Element Analysis (FEA) enables evaluation of robotic structures under realistic stress and deformation scenarios, ensuring mechanical safety during repetitive agricultural operations. Zhang et al. [15] designed a 5-DOF hybrid serial-parallel manipulator using a novel 2T1R planar parallel mechanism, followed by FEA-based topology optimization to reduce structural weight while maintaining high stiffness and modularity, making it suitable for sorting and packaging tasks. Zhang et al. [15]. Amir et al. [16] implemented FEA for a strawberry-picking arm tailored to plant geometry, confirming mechanical safety and validating workspace simulations via MATLAB. Amir et al. [16]. Bauer et al. [17] applied structural analysis to multi-material, 3D-printed soft end-effectors for soil and crop interaction, validating their strength and durability despite low-cost fabrication. Bauer et al. [17]. Wang and Fan [18] introduced a bionics-inspired gripper with adjustable PVDF-based force sensing and validated its structure using FEA and Adams simulation, achieving a $23.2 \pm 5\%$ reduction in fruit damage during picking. Wang and Fan [18]. Li and Li [13] incorporated FEA-driven optimization into robotic arm design to enhance weight efficiency without compromising load capacity, optimizing link geometry under multi-axial loading and environmental stress. [14]. For capsicum harvesting robots, applying FEA under conditions such as grip force application, canopy collision, and long-term load cycles provides critical insights for reinforcement of joints, material selection (e.g., PLA+), and structural wall thickness calibration to prevent field failures.

Kinematic modeling plays a pivotal role in robot motion planning, workspace validation, and collision-free trajectory generation, particularly in constrained agricultural settings. Wang et al. [19] developed a ROS-based simulation and control system for a dual-arm tomato harvesting robot, employing URDF for modeling, RViz and MoveIt! for motion planning, and integrating ROS-based vision and serial communication modules for precise localization Wang et al. [19]. Sepúlveda et al. [20] proposed a dual-arm ROS-compatible platform using 6-DOF Kinova MICO™ manipulators and RGB-Depth cameras, allowing environment-aware motion control and perception evaluation in unstructured farming scenarios Sepúlveda et al. [20]. Chen and Liu [21] implemented a ROS-based grasping robot system with real-time control via RViz, demonstrating high reliability and responsiveness in simulated and real part-handling tasks Chen and Liu [21]. Van Herck et al. [8] emphasized singularity avoidance and obstacle-aware motion planning in greenhouse robotics using forward and inverse kinematic models [8]. Modern approaches integrate kinematic modeling with real-time joint feedback from sensors like potentiometers or encoders to fine-tune pose estimation and improve simulation fidelity. ROS-based simulation environments like Gazebo or MoveIt! enable validation of joint trajectories, grasp-pose generation, and manipulability mapping before physical prototyping. These frameworks significantly reduce real-world trial needs, particularly when addressing occlusion, fruit clustering, and peduncle localization in capsicum harvesting.

From the above literature, it is evident that although robotic systems for agricultural applications have seen significant advancements, there exists a specific gap in the mechanical and simulation-driven design of manipulators tailored for greenhouse capsicum harvesting. Current systems often generalize structural design without explicitly mapping the morphological traits of capsicum plants such as clustered fruit orientation, flexible peduncles, and narrow canopy architecture into design constraints, thereby limiting harvesting efficiency and safety. Additionally, while several robotic arms have been structurally analyzed, a detailed finite element analysis (FEA) of each link under fruit-specific load conditions using lightweight 3D-printable materials like Polylactic Acid Plus (PLA+) remains underexplored. Furthermore, most simulation frameworks either lack ROS 2 integration or provide limited validation

of workspace coverage and motion planning strategies customized for capsicum picking. Hence, there is a pressing need for a comprehensive study that integrates mechanical CAD-based design, FEA-driven structural validation, and ROS 2-based kinematic simulation for a 6-DOF robotic arm optimized for capsicum harvesting in greenhouse environments.

Based on this justification, the present study is structured around the following objectives.

1. **Mechanical Design:** To design a lightweight, modular 6-DOF robotic arm for greenhouse capsicum harvesting, integrating plant-specific traits such as fruit height, canopy spread, stem flexibility, and occlusion into mechanical constraints.
2. **Structural Analysis:** To perform FEA-based structural validation of the robotic arm under harvesting loads, ensuring safe operation by analyzing stress, deformation, and factor of safety for PLA+ components.
3. **Kinematic Simulation:** To implement kinematic modeling and simulate motion planning using ROS 2, RViz2, and MoveIt2, validating reachability, joint trajectories, and workspace coverage for capsicum harvesting.

This research adopts a structured methodology to address the design, validation, and simulation of a 6-DOF robotic arm tailored for capsicum harvesting in greenhouse environments. The paper begins with the **Introduction**, which outlines the growing need for automation in precision horticulture, identifies the morphological challenges posed by *Capsicum annuum* (e.g., clustered fruits, stem flexibility, occlusions), and highlights current research gaps in manipulator design and simulation-driven validation. Section 2: Materials and Methods presents a crop-informed engineering approach, starting from the greenhouse cultivation of the Arka Athulya capsicum variety to extract plant-specific parameters for kinematic design. The section then details the CAD modeling of a modular robotic manipulator in SOLIDWORKS, followed by structural safety validation using Finite Element Analysis (FEA) under part-wise loading scenarios. It further introduces forward kinematic modeling using the Denavit–Hartenberg convention and elaborates on the ROS 2-based simulation framework using URDF file generation, MoveIt 2 for motion planning, and RViz 2 for trajectory visualization and workspace coverage analysis. Section 3: Results and Discussion presents the FEA output, including stress, displacement, and factor of safety results for PLA+ structures, followed by ROS 2 simulation outcomes such as pose estimation accuracy, joint-angle time profiles during fruit approach and grasp, end-effector reachability spheres, and coverage of capsicum harvesting zones. Gripper simplification for URDF export and actuation simulation is also addressed. Section 4: Conclusions summarizes the efficacy of the proposed manipulator design and ROS-based simulation pipeline, discusses its potential deployment readiness, and suggests directions for future enhancements. The paper concludes with a References section citing all supporting literature and simulation tools.

2. MATERIALS AND METHODS

2.1. Cultivation of Capsicum for Robotic Arm Design and Kinematics

To establish a biologically grounded framework for robotic manipulator design, workspace evaluation, and inverse kinematic modeling, *Capsicum annuum* (*cv. Arka Athulya*) was cultivated under controlled conditions in a naturally ventilated greenhouse at the Agricultural and Food Engineering Department, Indian Institute of Technology Kharagpur (**Figure 1**). This experimental cultivation served as a critical step for acquiring detailed morphological, spatial, and mechanical data of the plant canopy essential for accurate robotic configuration. The *Arka Athulya* variety, characterized by uniform fruit morphology, sturdy peduncles, and a compact growth habit, was specifically chosen to support reliable robotic harvesting interactions. The sowing process began in October 2024, with seedlings initially raised in trays for a period of 30 days before transplanting onto structured raised beds arranged in a paired-row layout. A consistent inter-row spacing of 0.45 m and intra-row plant spacing of 0.40 m was maintained to establish a predictable canopy structure with defined occlusion zones and fruit distribution patterns. Raised beds measured 0.9 m in width and 0.15 m in height, with 1 m spacing between adjacent beds, ensuring sufficient clearance for robotic base mobility and arm articulation. The sandy loam soil type was selected to promote healthy

root development and maintain optimal plant physiology throughout the cropping cycle. This controlled and standardized cultivation setup (Table 1) enabled systematic capture of plant geometry and spatial variability, which directly informed the determination of joint range limits, reachable workspace volumes, and pose estimation parameters critical to the robotic arm's structural and kinematic design.



Figure 1. Greenhouse cultivation of *Capsicum annuum* for robotic arm design.

Table 1. Cultivation parameters for capsicum in greenhouse.

Parameter	Details
Cultivar used	<i>Arka Athulya</i>
Fruit color	Green
Sowing method	Seedlings raised in portrays
Planting layout	Paired row configuration
Inter-row spacing	0.45 m
Intra-row spacing	0.40 m
Raised bed size (W × H)	0.9 m × 0.3 m
Bed-to-bed spacing	1 m
Soil type	Sandy loam
Cultivation period	Winter (Nov 2024 – March 2025)
Harvest window	75–85 days post-transplantation
Total crop duration	5 – 6 months

2.2. Design Considerations Based on *Capsicum* Plant Morphology

Leveraging the structured greenhouse cultivation parameters outlined in Section 2.1, the robotic arm's structural and kinematic configuration was systematically tailored based on the morphological characteristics and spatial organization of *Capsicum annuum* plants under real cultivation scenarios. These plant-specific attributes served as critical determinants in defining the manipulator's geometric constraints, joint articulation strategy, and mechanical design limits.

As presented in Table 2, essential geometric metrics including bed width (0.90 m), plant height range (0.60–1.00 m), and canopy spread (0.30–0.60 m), directly influenced the robot's reachable workspace and the required degree of freedom (DOF) configuration. The narrow inter-plant spacing (0.40 m) and clustered canopy structure necessitated a compact arm footprint with enhanced lateral flexibility, optimized for integration onto mobile platforms navigating confined greenhouse aisles. The fruit-bearing zone, typically located 0.30–0.80 m above the ground, dictated vertical reachability and end-effector trajectory constraints, especially when addressing occluded or partially visible fruit clusters containing 2–5 fruits per node. Payload considerations, derived from the average fruit mass (120–180 g), informed actuator sizing and gripper compliance thresholds to ensure efficient yet non-damaging harvesting operations.

Further, the mechanical interaction dynamics during harvesting were defined through an evaluation of stem and peduncle biomechanics, detailed in Table 3. The stem exhibits moderate stiffness and elastic recovery, which necessitates a compliant and adaptive motion profile across joints to prevent structural damage to the plant. Given

the constraint that maximum permissible contact forces must remain below 10 N, fine-tuned force control and real-time collision avoidance become imperative for safe operation. These biomechanical insights guided critical design decisions such as lightweight material selection, joint torque specifications, and smooth trajectory generation. Collectively, these parameters informed the development of a biologically compatible and functionally robust robotic arm capable of autonomous capsicum harvesting in spatially constrained greenhouse environments.

Table 2. Geometric and structural parameters of capsicum plants relevant to robotic manipulator design.

Parameter	Value	Design Implication
Greenhouse bed width	90 cm	Constrains the base frame and lateral mobility of the robot; impacts mounting feasibility.
Plant height	60–100 cm	Sets the minimum vertical reach requirement to access fruit across canopy layers.
Canopy spread (Width & depth)	30–60 cm	Defines operational workspace boundaries for the end-effector; critical for collision-free movement.
Intra-row plant spacing	40 cm	Demands compact link dimensions and a reduced turning radius for maneuverability in narrow gaps.
Branch count and growth pattern	6–10 branches, radial orientation	Influences joint configuration for collision avoidance and trajectory optimization.
Fruit height from ground	30–80 cm	Guides end-effector positioning and approach angles for efficient harvesting.
Average fruit mass	120–180 g	Used for payload estimation, actuator torque selection, and gripper force calibration.
Occlusion level of peduncle/Fruit	High in dense canopy	Necessitates vision-based pose estimation and multi-DOF arm articulation.
Fruit cluster density	2–5 fruits per node	Demands precision manipulation and high dexterity to avoid damage during selective picking.

Table 3. Mechanical interaction characteristics of capsicum plants influencing manipulator design.

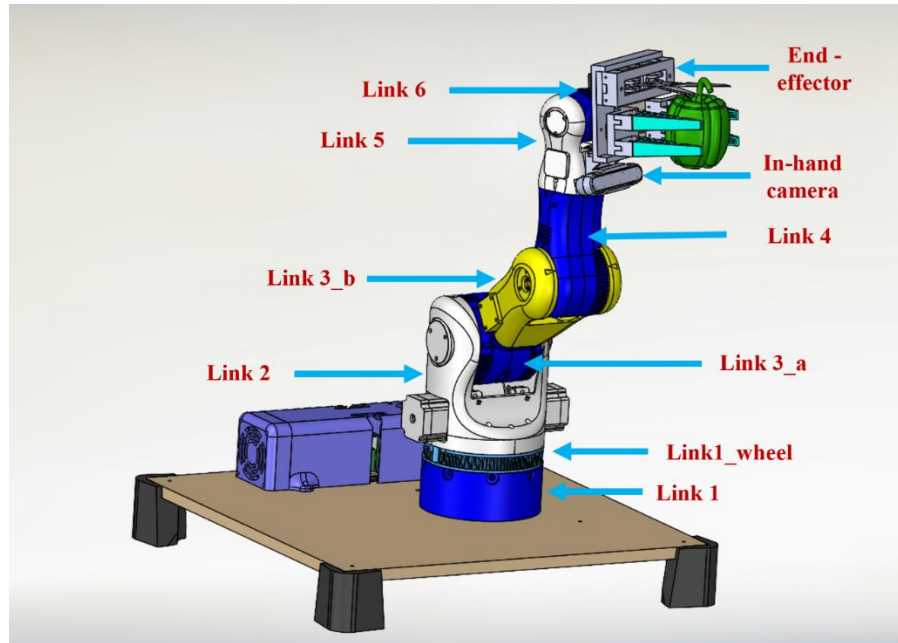
Parameter	Value	Design Implication
Stem and branch flexibility	Medium to high	Requires compliant motion strategies and joint-level adaptability to avoid plant damage.
Max. permissible contact force	< 10 N	Dictates end-effector force thresholds for safe fruit engagement and detachment.
Stiffness and recovery response	Moderate with fast rebound	Informs damping design and control logic for safe impact handling and responsive motion control.

2.3. Structural Design of the Robotic Manipulator

Taking into account the spatial limitations and biological characteristics of capsicum plants outlined in Section 2.2, a six-degree-of-freedom (6-DOF) articulated robotic manipulator was structurally designed using SOLIDWORKS Premium 2022 (Dassault Systèmes, Vélizy-Villacoublay, France) [22]. The design prioritized lightweight construction, modularity, and the ability to effectively navigate within greenhouse canopies. The robot adopts a serial-link configuration consisting of seven primary links, including the wrist and end-effector, with joint trajectories optimized for operation within a confined canopy spread of 30–60 cm and plant height envelope of 60–100 cm (Figure 2). For prototyping, the structural links were fabricated via Fused Deposition Modeling (FDM) using Polylactic Acid Plus (PLA+), selected for its balance of stiffness and ease of manufacturing. The end-effector employed a hybrid-material strategy: gripper elements were constructed from flexible Thermoplastic polyurethane (TPU) (Shore hardness 85A) to ensure compliant fruit engagement, while the integrated scissor-based cutting mechanism was fabricated from stainless steel to enable reliable peduncle severing. This multi-material approach enabled a low-mass manipulator with a rated payload capacity of 200 g, adequate for handling capsicum fruits typically weighing between 120–180 g, along with the attached end-effector assembly. The dimensional specifications and material allocation for each robotic link are summarized in Table 4, based on the final prototype measurements.

Table 4. Link-wise dimensions, materials, and weights of the capsicum harvesting robotic arm.

Link No.	Function	Material	Length (mm)	Weight (kg)
Link 1	Base mounting	PLA+	70	0.45
Link1_wheel	Support above base	PLA+	20	0.15
Link 2	Shoulder joint	PLA+	200	0.50
Link 3_a	Upper arm (Segment A)	PLA+	140	0.40
Link 3_b	Upper arm (Segment B)	PLA+	190	0.35
Link 4	Elbow joint	PLA+	175	0.30
Link 5	Forearm	PLA+	130	0.10
Link 6	Wrist pitch/Roll	PLA+	75	0.05
Link 7	End-effector + cutter	PLA+/TPU/SS	130	0.45

**Figure 2.** CAD model of the robotic arm with end-effector for capsicum harvesting.

2.4. Structural Analysis of Designed Robotic Manipulator

Building upon the structural configuration described in Section 2.3, the mechanical robustness of the designed 6-DOF articulated robotic arm was evaluated through Finite Element Analysis (FEA) using SolidWorks Simulation (Premium 2022, Dassault Systèmes, France) [22]. FEA enables the prediction of stress distribution (Equation 1), deformation (Equation 2), and structural performance under operational loading conditions, which is critical for validating the safety (Equation 3) and reliability of the robotic system prior to deployment. SolidWorks Static Simulation module was employed to assess the structural integrity of each individual link rather than the entire assembly to allow for isolated evaluation under relevant cumulative loading, simplify constraint definition, and reduce meshing complexity. The simulation setup specifications are summarized in Table 5, which outlines solver type, mesh strategy, and analysis metrics such as Von Mises stress and total displacement.

$$\sigma_{vm} = \sqrt{\frac{(\sigma_1 - \sigma_2)^2 + (\sigma_2 - \sigma_3)^2 + (\sigma_3 - \sigma_1)^2}{2}} \quad (1)$$

$$\delta = \frac{F \cdot L}{A \cdot E} \quad (2)$$

$$FoS = \frac{\sigma_{max}}{\sigma_{yield}} \quad (3)$$

Where:

- σ_{vm} = Von Mises Stress.

- δ = Total Linear Deformation.
- FoS = Safety Factor.
- $\sigma_1, \sigma_2, \sigma_3$ = Principal stresses.
- δ = Linear deformation (m).
- F = Applied axial force (N).
- A = Cross-sectional area (m²).
- L = Length of the link (m).
- E = Young's modulus of the material (Pa).
- σ_{yield} = Yield strength of material (Pa).
- σ_{max} = Maximum simulated Von Mises stress (Pa).

The FEA process consisted of four key steps for each link: (i) assignment of appropriate material properties based on the component function and manufacturing feasibility, (ii) application of fixture constraints to simulate physical mounting or joint anchoring conditions, (iii) application of external loads computed from cumulative mass above each link, and (iv) meshing using the Standard Mesh algorithm with curvature-based refinement for improved accuracy.

To ensure realistic simulation fidelity, material definitions were applied based on actual component fabrication, as shown in Table 6. Rigid links (base to wrist) were assigned PLA+ due to its lightweight nature and acceptable strength-to-weight ratio for 3D-printed components, while the compliant fingers of the end-effector were modeled with TPU (Shore 85A) for flexibility. The cutting interface utilized stainless steel to withstand shearing forces during peduncle removal.

Material parameters, including elastic modulus, yield strength, Poisson's ratio, and density were incorporated into the simulation to model accurate deformation and failure thresholds. The mechanical loading was determined through a bottom-up approach, accounting for cumulative weight and force transmission through the robotic chain during harvesting operations.

As detailed in Table 7, individual components such as Link 2 (shoulder), Link 3 (arm segments), and Link 8 (end-effector) were subjected to their corresponding axial and lateral loads derived from gravitational force calculations. Load directionality was aligned with expected working conditions: vertically downward for gravity loads and inward/outward vectors based on actuation axis and fruit access strategy. Boundary conditions (fixtures) were assigned at realistic mounting faces (e.g., fixed base flange, joint-to-joint interfaces), and standard meshing was employed for reliable convergence.

This structural analysis pipeline validated that all robotic arm components fall within acceptable stress limits under expected harvesting loads, and guided iterative reinforcement of critical links such as the forearm and wrist. These insights directly informed material choices and design tolerances, ensuring that the robotic arm not only meets spatial and kinematic constraints from Section 2.2 but also withstands the mechanical demands of greenhouse harvesting.

Table 5. Software setup for static simulation in SOLIDWORKS.

Parameter	Specification
Cad software	SOLIDWORKS Premium 2022
Simulation type	Static Structural
Gravity enabled	Yes (9.81 m/s ²)
Mesh type	Standard Mesh (Curvature-based)
Solver	FFEPlus (iterative)
Result metrics	Von Mises stress, displacement, FOS

Table 6. Material properties used for FEA simulation.

Property	PLA+	TPU (Shore 85A)	Stainless Steel (304)
Young's Modulus (MPa)	3450	26	200,000
Poisson's Ratio	0.36	0.48	0.30
Density (kg/m ³)	1240	1200	8000
Yield Strength (MPa)	50	7.89	250
Ultimate Tensile Strength (MPa)	65	8.5	505
Thermal Expansion (1/K)	68e-6	160e-6	17.2e-6
Damping Ratio (Structural)	Low	Moderate	Low
Behavior	Rigid-Plastic	Hyperelastic-like	Rigid-Elastic

Table 7. Link-wise simulation setup for FEA in SOLIDWORKS.

Link no.	Component name	Material	Applied force (N)	Load direction	Fixture condition
1	Link 1 (Base)	PLA+	26.98	Vertical downward	Fixed at bottom face (Mount to platform)
2	Link 1_w (Wheel after Base)	PLA+	22.56	Vertical downward	Fixed concentrically to base flange.
3	Link 2 (Shoulder)	PLA+	21.09	Downward & inward	Fixed at joint with Link 1
4	Link 3_a (Lower Arm)	PLA+	16.19	Downward & inward	Fixed to Link 2 interface
5	Link 3_b (Upper Arm)	PLA+	12.26	Downward & inward	Fixed to Link 3_a connection
6	Link 4 (Elbow)	PLA+	8.83	Downward & inward	Fixed to Link 3_b joint
7	Link 5 (Forearm)	PLA+	5.89	Downward & inward	Fixed to Link 4 connection
8	Link 6 (Wrist)	PLA+	4.91	Downward & inward	Fixed to Link 5 connection
9	Link 8 (End-effector)	PLA+/TPU/SS	4.41	Downward & outward	Fixed at wrist interface (Link 6)

2.5. Kinematic Modeling and ROS 2-Based Simulation Framework

To validate the reachability, workspace constraints, and joint-level articulation of the designed capsicum harvesting manipulator, forward kinematic modeling and ROS 2-based simulation were implemented. Forward kinematics provides the pose of the end-effector (position and orientation) given the joint parameters and is fundamental in evaluating the manipulator's capability to reach spatial targets under joint and structural constraints. This was essential for confirming whether the robotic arm could effectively navigate the wide canopy and tall plants described earlier in Section 2.3. The Denavit–Hartenberg (DH) parameterization method was used to model the 6-DOF serial-link configuration, where each transformation between two consecutive joints was defined by four parameters: link length, link twist, link offset, and joint angle. The complete DH parameter set used in this study is summarized in Table 8.

The simulation architecture was built on ROS 2 Humble [23] using RViz2 and MoveIt2 for motion planning. The robotic arm's mechanical structure, defined through the SolidWorks CAD model, was converted into a Unified Robot Description Format (URDF) (Figure 3) to enable integration with ROS tools. Each link was exported as an STL mesh and referenced in the URDF using and tags. The inertial data were calculated from link-wise physical properties obtained through Section 2.4's FEA analysis. All joints were defined as revolute with appropriate axis orientation and motion limits, derived from task-specific velocity requirements and load-based constraints. The joint-level actuation specifications critical for motion planning are provided in Table 9, including the functional purpose, practical RPM range, and rationale for each joint's design.

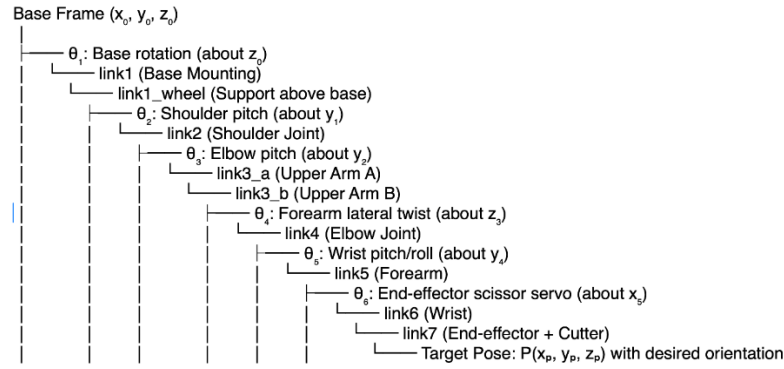


Figure 3. Robotic arm URDF structure.

To simulate robot behavior and test kinematic feasibility, a new ROS 2 package named `capsicum_arm_description` was created within the workspace `ws_gazebo`, containing the URDF, Xacro, and mesh resources. Launch files were developed using `robot_state_publisher`, `joint_state_publisher_gui`, and `RViz2` configurations to visualize and manually actuate the robotic joints. The forward kinematics and collision-free path validation were achieved through `MoveIt2`, which was initialized using the `MoveIt Setup Assistant`. This setup allowed the definition of planning groups, end-effectors, kinematic solvers, and motion constraints specific to the greenhouse harvesting context. The final `MoveIt2` planning interface supported inverse kinematics computations, joint-space planning, and Cartesian path generation. Importantly, joint constraints and workspace boundaries defined from real plant geometry were encoded in the SRDF collision matrix and planning configuration, ensuring biologically compatible motion.

Table 8. Denavit–Hartenberg Parameters for the 6-DOF robotic manipulator.

Joint	a_l (mm)	α_l (deg)	d_l (mm)	θ_l (variable)
J1	0	90	65	θ_1
J2	200	0	0	θ_2
J3	140	0	0	θ_3
J4	190	90	0	θ_4
J5	175	90	0	θ_5
J6	130	0	0	θ_6

Table 9. Joint specifications and RPM constraints for simulation and motion planning.

Joint (Link)	Joint Type	Function	RPM	Reason
Base (J1)	Revolute	Yaw rotation of the full arm	10–20	Enables stable sweeping motion of the full arm.
Shoulder (J2)	Revolute	Main lifting arm	10–30	Requires more torque and slower, controlled lift.
Elbow (J3)	Revolute	Bending forearm	15–35	Allows faster arm folding for reach.
Wrist 1 (J4)	Revolute	Pitching of wrist	20–50	Lightweight, allows rapid orientation.
Wrist 2 (J5)	Revolute	Rolling of wrist	20–50	Aids in dexterous manipulation
Gripper (J6)	Revolute	Scissor/cutting mechanism	30–60	Requires fast, responsive actuation.

Table 10. ROS 2 and simulation tool specifications.

Tool	Version/Specification	Function
ROS 2	Humble Hawksbill (Ubuntu 22.04)	Core middleware for robotic system integration
RViz2	Default with ROS 2 Humble	3D visualization of robot state and sensors
MoveIt2	Binary install from ROS 2 repo	Motion planning, FK/IK, collision detection
URDF/Xacro	XML and macro format	Robot description and modular link modeling
STL Files	Exported from SolidWorks	Link geometry used for visual/collision modeling
Joint State GUI	ROS GUI tool	Manual testing of joint limits and articulation

The complete ROS 2–MoveIt2–RViz2 pipeline enabled real-time simulation of peduncle-approach trajectories, reachability analysis, and motion validation without the need for physical trials. The specifications for ROS 2 packages

and tools used in this simulation setup are consolidated in Table 10, establishing the simulation stack as a reproducible and scalable framework for field-ready agricultural robotic systems.

This integrated simulation architecture ensures that the designed manipulator can be rigorously evaluated in a virtual environment before hardware deployment, with joint-level motion planning, spatial reach validation, and real-time visualization aligned with the biological and mechanical constraints identified in Sections 2.2 to 2.4.

3. RESULTS AND DISCUSSION

3.1. FEA Analysis Results of Designed Robotic Manipulator

Following the structural modeling and mechatronic integration methodology described in Section 2.3, Finite Element Analysis (FEA) was performed on each individual link of the robotic manipulator to evaluate mechanical safety under operational loads. The simulations were conducted using SolidWorks Simulation (Premium 2022, Dassault Systèmes, France), leveraging the static analysis environment with standard meshing settings and isotropic linear material properties corresponding to PLA+ for primary structural links, and TPU and Stainless Steel for the gripper segment. The analysis was carried out independently for each link, as opposed to full-assembly simulation, to improve computational efficiency and isolate stress distribution profiles under localized loading, based on the vertical and directional load values previously calculated in Table 8.

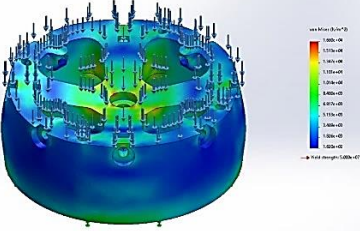
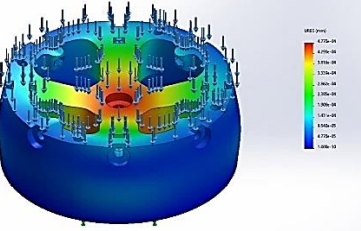
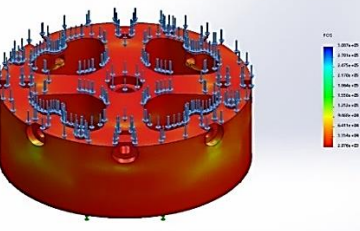
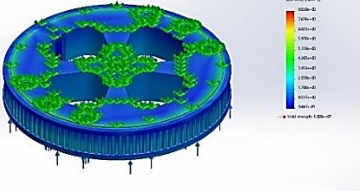
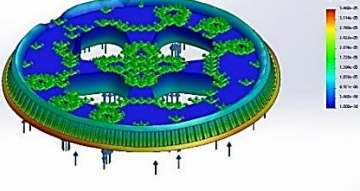
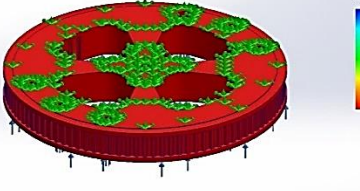
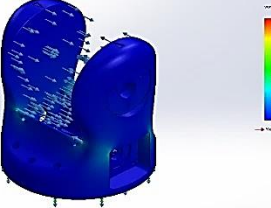
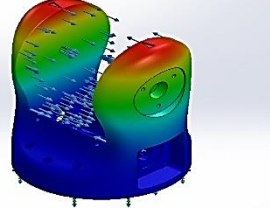
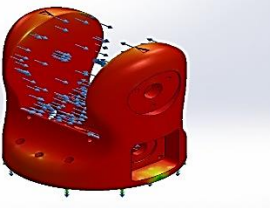
The FEA results are consolidated in Table 11, which reports the von Mises stress, total displacement, and Factor of Safety (FoS) for all nine primary components of the manipulator. The highest stress concentration was observed in Link 2, which carries the largest cumulative load (21.09 N), registering a maximum stress of 5.644×10^5 Pa. This result aligns with the role of Link 2 as the shoulder joint, a critical load-bearing element that not only supports upper links but also handles significant bending torque during vertical movements. In contrast, the lowest stress of 8.529×10^3 Pa was found in Link 1_wheel, a stationary support component that contributes minimally to motion or payload distribution.

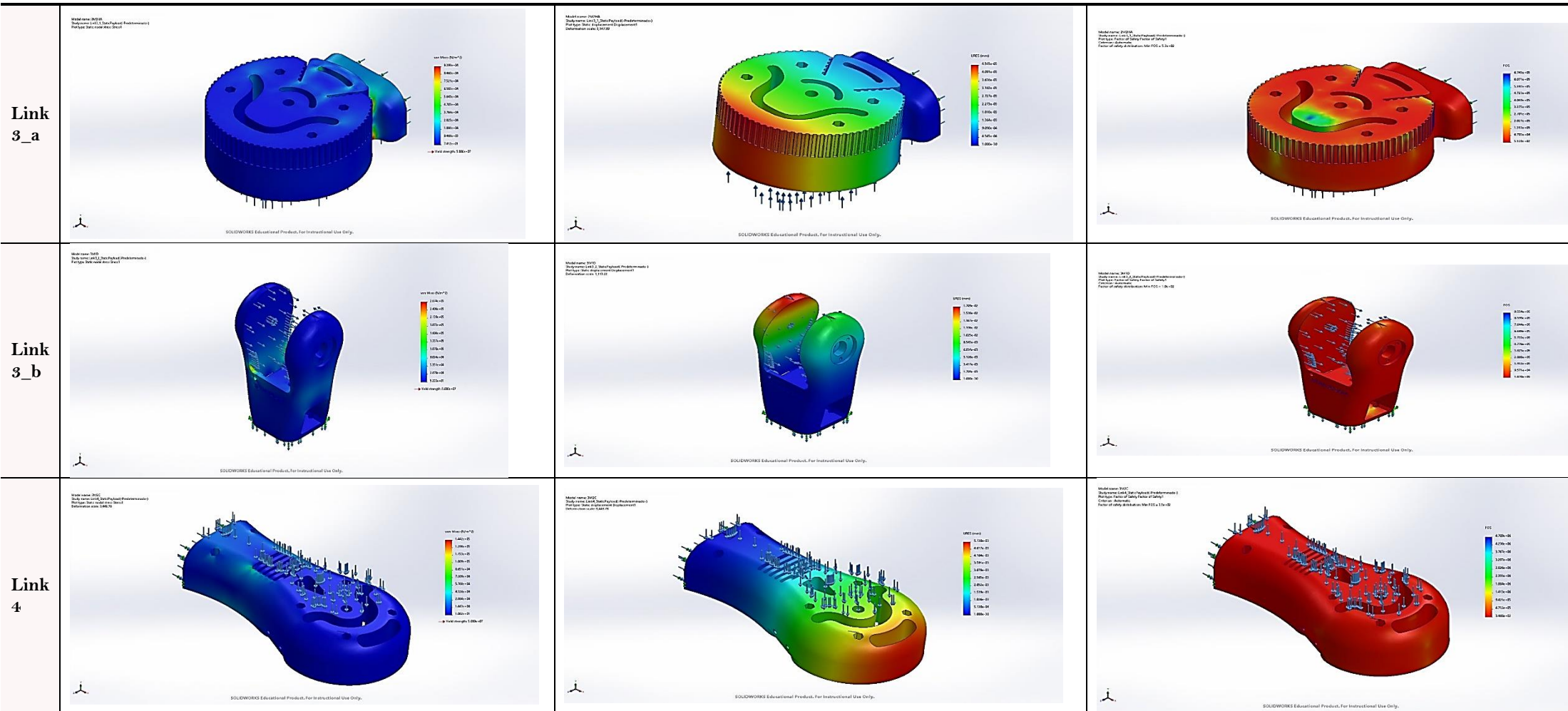
Regarding displacement, the highest value was recorded in Link 5 at 2.53×10^{-2} mm, likely due to its position at the distal end of the manipulator where accumulated flexural deflection from upper links is maximum. This displacement remains well within allowable deformation limits for PLA+, suggesting no risk of permanent structural deviation under operating conditions. The lowest displacement of 3.460×10^{-5} mm occurred in Link 1_wheel, which is fixed to the base with minimal external loading and experiences negligible stress propagation.

The Factor of Safety (FoS) values across all parts significantly exceeded critical thresholds, with the minimum FoS still being 88.58, again in Link 2, further confirming its criticality under load. Despite being the most stressed part, this FoS confirms a substantial safety margin when compared to the yield strength of PLA+ (reported as 50 MPa). These high FoS values are attributable to conservative material usage and the lightweight, modular design intended for low-payload capsicum harvesting operations. Emphasis was placed on PLA+ components due to their relatively lower stiffness and strength compared to metal counterparts. This allowed validation of the robot's structural feasibility even under worst-case scenarios, highlighting that even in these critical parts, material failure is highly unlikely. Stress and displacement contour plots for each component are illustrated in Table 11, with high-stress zones observed near joint interfaces, particularly in torque-sensitive links such as Link 2 and Link 3_a, emphasizing the importance of reinforcement in design.

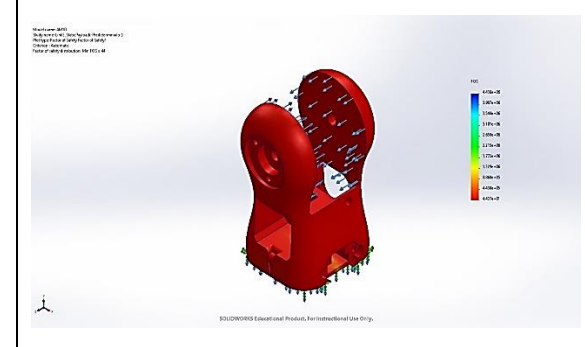
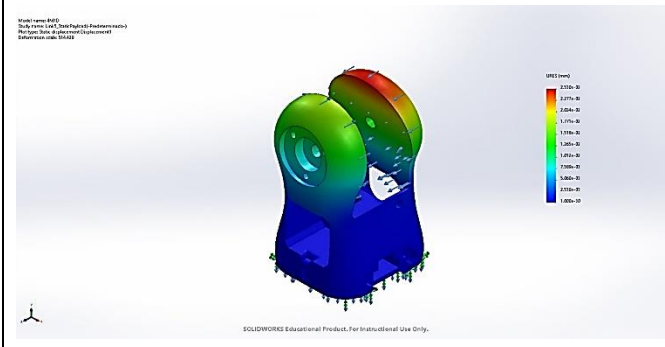
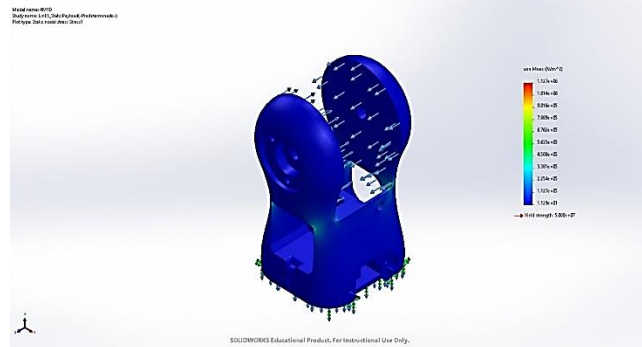
Hence, the FEA results confirm that the robotic manipulator, as designed and fabricated using PLA+ material, meets all structural safety requirements under expected loading conditions for capsicum harvesting. These insights guide future enhancements in actuator selection, material optimization, and topology refinement for advanced iterations of the system.

Table 11. FEA results for each manipulator link showing von Mises stress, displacement, and factor of safety.

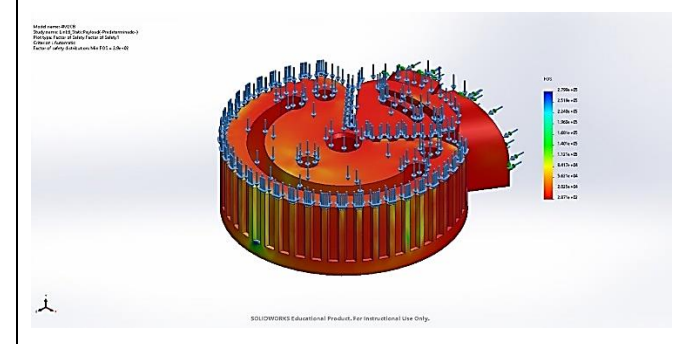
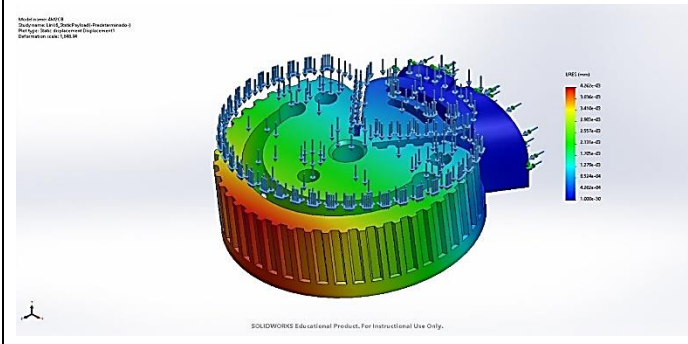
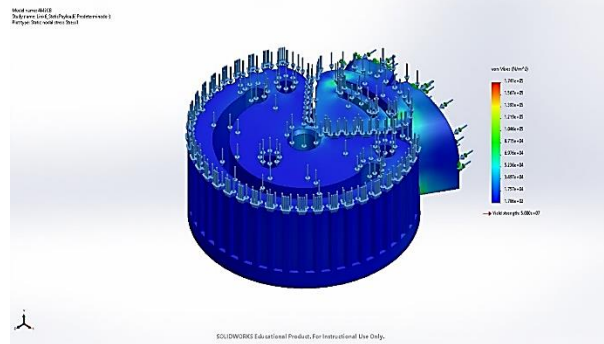
Link	Stress Plots	Displacement Plots	FoS Plots
Link 1	<p>Model Name: 12000 Part Name: Link 1 (SolidWorks Partname: 1) Analysis Type: Static Structural Simulation Date: 10/10/2024</p>  <p>von Mises (N/mm²) 1.000e-01 5.000e-02 0.000e+00</p> <p>→ Max Stress: 1.000e-01</p> <p>SOLIDWORKS Educational Product. For Instructional Use Only.</p>	<p>Model Name: 12000 Part Name: Link 1 (SolidWorks Partname: 1) Analysis Type: Static Structural Simulation Date: 10/10/2024</p>  <p>DISP (mm) 1.000e-01 5.000e-02 0.000e+00</p> <p>SOLIDWORKS Educational Product. For Instructional Use Only.</p>	<p>Model Name: 12000 Part Name: Link 1 (SolidWorks Partname: 1) Analysis Type: Static Structural Simulation Date: 10/10/2024</p>  <p>FoS 1.000e-01 5.000e-02 0.000e+00</p> <p>SOLIDWORKS Educational Product. For Instructional Use Only.</p>
Link 1_w	<p>Model Name: 12000 Part Name: Link 1 (SolidWorks Partname: 1) Analysis Type: Static Structural Simulation Date: 10/10/2024</p>  <p>von Mises (N/mm²) 1.000e-01 5.000e-02 0.000e+00</p> <p>→ Max Stress: 1.000e-01</p> <p>SOLIDWORKS Educational Product. For Instructional Use Only.</p>	<p>Model Name: 12000 Part Name: Link 1 (SolidWorks Partname: 1) Analysis Type: Static Structural Simulation Date: 10/10/2024</p>  <p>DISP (mm) 1.000e-01 5.000e-02 0.000e+00</p> <p>SOLIDWORKS Educational Product. For Instructional Use Only.</p>	<p>Model Name: 12000 Part Name: Link 1 (SolidWorks Partname: 1) Analysis Type: Static Structural Simulation Date: 10/10/2024</p>  <p>FoS 1.000e-01 5.000e-02 0.000e+00</p> <p>SOLIDWORKS Educational Product. For Instructional Use Only.</p>
Link 2	<p>Model Name: 12000 Part Name: Link 2 (SolidWorks Partname: 1) Analysis Type: Static Structural Simulation Date: 10/10/2024</p>  <p>von Mises (N/mm²) 1.000e-01 5.000e-02 0.000e+00</p> <p>→ Max Stress: 1.000e-01</p> <p>SOLIDWORKS Educational Product. For Instructional Use Only.</p>	<p>Model Name: 12000 Part Name: Link 2 (SolidWorks Partname: 1) Analysis Type: Static Structural Simulation Date: 10/10/2024</p>  <p>DISP (mm) 1.000e-01 5.000e-02 0.000e+00</p> <p>SOLIDWORKS Educational Product. For Instructional Use Only.</p>	<p>Model Name: 12000 Part Name: Link 2 (SolidWorks Partname: 1) Analysis Type: Static Structural Simulation Date: 10/10/2024</p>  <p>FoS 1.000e-01 5.000e-02 0.000e+00</p> <p>SOLIDWORKS Educational Product. For Instructional Use Only.</p>



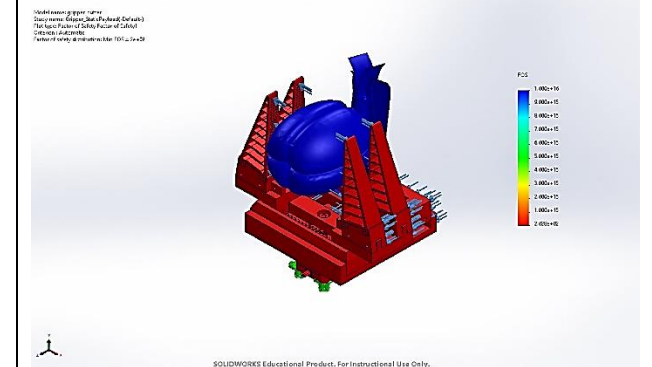
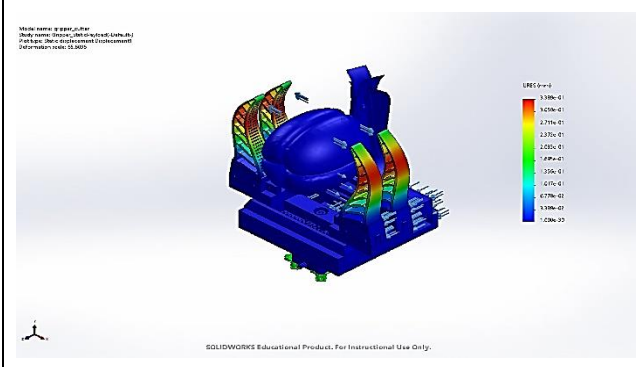
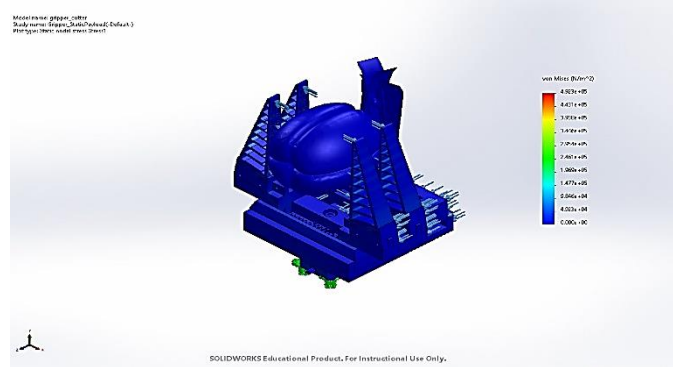
Link
5



Link
6



Link
7



3.2. ROS 2-Based Simulation Results

To evaluate the performance, reachability, and practical motion feasibility of the developed 6-DOF harvesting manipulator, a detailed simulation study was conducted based on the ROS 2 framework, as described in Section 2.5. The robotic model was implemented using URDF derived from the CAD geometry and simulated within MoveIt2 and RViz2 environments. For improved compatibility with simulation tools and to streamline the exportation process, the original end-effector with an integrated scissor mechanism was simplified into a parallel-jaw gripper. This abstraction preserved the essential grasping function while minimizing complexity in mesh handling and frame association during motion planning. Figure 4 shows the planning scene as visualized in RViz2, where the manipulator model is rendered with proper joint hierarchy, link geometries, and interactive planning markers. The coordinate frames for each joint are correctly aligned, confirming successful construction of the kinematic chain. The MoveIt2 interface was used to configure motion groups, validate forward kinematics, and generate collision-free paths between target poses. The gripper, represented with a simplified closing mechanism, was able to simulate basic approach and pick actions needed for harvesting tasks.

The actuator-level behavior of the robot was further analyzed through the joint angle evolution over time, reflecting a full motion cycle from base rotation to fruit grasping. Figure 5 illustrates the angular displacement of each revolute joint (θ_1 to θ_6) over a 6-second period. The trajectory begins with θ_1 executing a base rotation of approximately 45° , positioning the arm toward the target location. This is followed by a shoulder pitch (θ_2) and elbow extension (θ_3), which lift and extend the arm into the workspace. Notably, the joints are activated in a sequential and phase-wise manner, indicating task-specific decoupling that reduces dynamic interaction and control complexity. The wrist joints (θ_4 and θ_5) contribute to orienting the end-effector appropriately, while the final joint (θ_6), which controls the gripper, activates rapidly at around 5 seconds coinciding with the moment of fruit capture. The joint profiles verify that the manipulator operates within its defined kinematic and dynamic constraints while executing a realistic harvesting sequence.

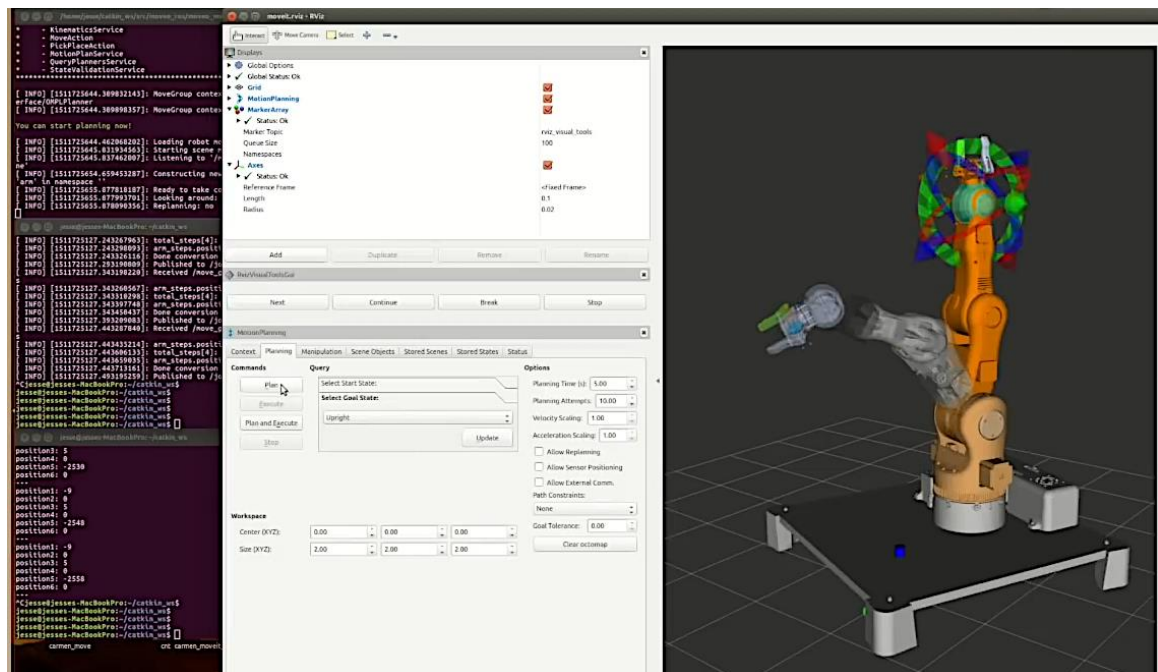


Figure 4. ROS 2 RViz visualization of the robotic arm model with simplified end-effector in MoveIt2.

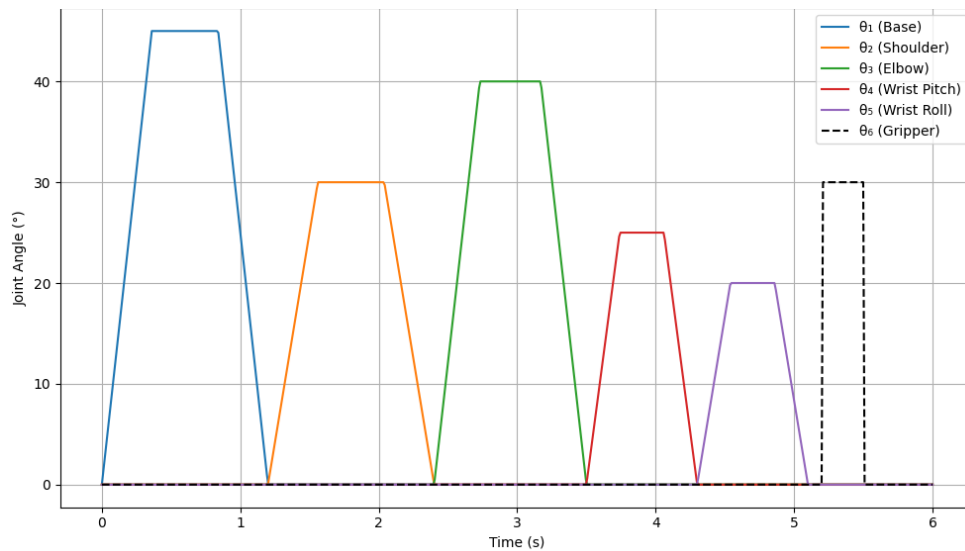


Figure 5. Joint angle profiles for the full 6-DOF manipulator during a single harvesting motion cycle.

To evaluate the positional fidelity of the forward kinematics model, 20 spatial poses were sampled across the robot's reachable workspace. The position error between the computed end-effector pose and the expected target was recorded, as shown in Figure 6. The error varied between 1.8 mm and 2.8 mm, with a mean value around 2.3 mm. These small deviations demonstrate that the DH-parameter-based transformation model used in the simulation closely approximates the true spatial configuration, ensuring that the end-effector can be reliably positioned within biologically tolerable limits. The observed variation is attributable to minor mesh misalignments and cumulative transformation inaccuracies but remains within acceptable thresholds for agricultural applications, where fruit peduncles typically allow for a few millimeters of positional flexibility.

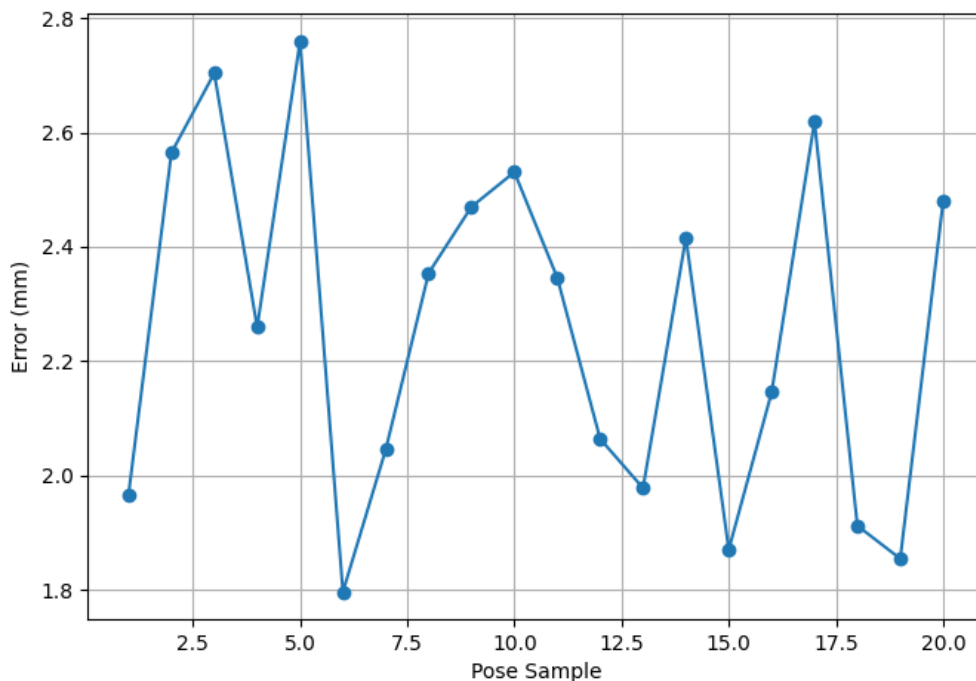


Figure 6. End-effector position error from forward kinematics across 20 target pose samples.

The planar reachability of the manipulator was visualized using a normalized polar plot as depicted in Figure 7. The reachability envelope represents the maximum radial extent the end-effector can achieve at various angles. The shape of the envelope is slightly asymmetric, reflecting the influence of joint angle limits and differing link lengths.

Despite these variations, the manipulator exhibits near-complete circular coverage, demonstrating its potential to access targets in all lateral directions. Such comprehensive reach is vital for operations in irregular and multi-layered plant canopies where fruits may appear at varying azimuthal positions.

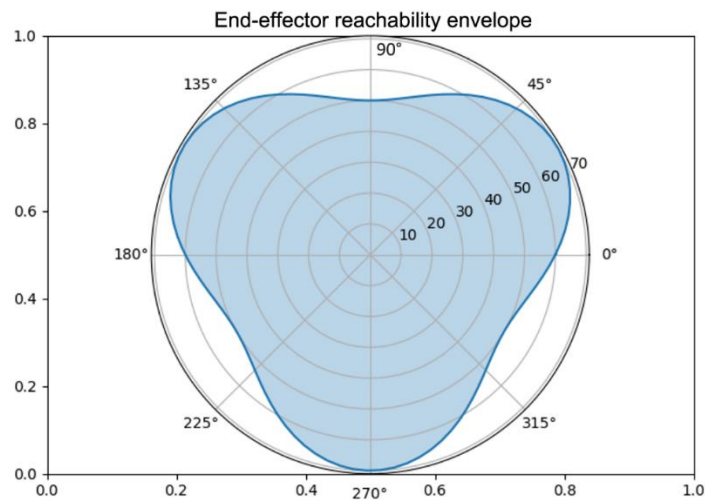


Figure 7. End-effector polar reachability envelope visualized in normalized radial units.

In three-dimensional space, the extent of the manipulator's reachable volume was compared with the expected fruit-bearing canopy coverage typical of capsicum plants. Figure 8 shows this volumetric overlay, with the outer blue region representing the full manipulator reach (~ 0.70 m) and the inner green region denoting the plant canopy coverage (0.40 m). The spatial overlap confirms that the robot is not only capable of reaching all desired fruit locations but also has additional margin for obstacle avoidance and approach optimization. This analysis establishes that the manipulator's workspace has been well-matched to the biological domain it is designed to serve.

Collectively, these results confirm that the proposed manipulator design, its simplified end-effector configuration, and the ROS 2-based simulation framework form a reliable and biologically compatible platform for greenhouse fruit harvesting. The integration of mechanical, kinematic, and computational considerations within this simulation pipeline allows for effective pre-deployment testing, reducing the risk and cost associated with field-level trials.

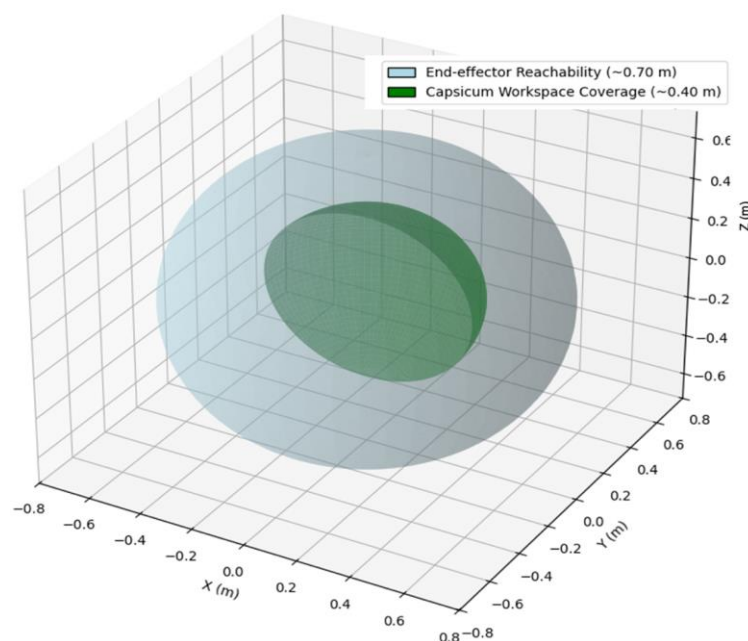


Figure 8. Workspace comparison showing total manipulator reachability and capsicum canopy coverage.

4. CONCLUSIONS

This research presents an integrated framework for the design, structural validation, and motion planning simulation of a 6-DOF robotic arm tailored for capsicum harvesting in structured greenhouse environments. Firstly, a modular and lightweight manipulator was designed based on the spatial and morphological characteristics of capsicum plants, such as canopy spread, fruit positioning, stem flexibility, and occlusion patterns, ensuring crop-structure compatibility in mechanical design. Then, finite element analysis was conducted on each link to assess stress distribution, deformation, and factor of safety under representative harvesting loads, confirming the structural integrity of the PLA+ and multi-material components. Finally, a forward kinematic model was developed using the Denavit–Hartenberg convention and integrated into a ROS 2-based simulation environment. The robot was modeled in URDF and visualized in RViz2 and MoveIt2 to evaluate motion feasibility, workspace coverage, and joint trajectories. The generated results verified that the system can safely and effectively operate within greenhouse constraints, demonstrating its suitability for precision horticultural automation.

The following key conclusions summarize the technical achievements of the study.

1. A 6-DOF articulated robotic arm was mechanically designed using a hybrid-material approach involving PLA+, TPU (Shore hardness 85A), and stainless steel to meet the spatial and structural requirements of greenhouse-grown capsicum plants. The serial-link configuration was optimized for maneuvering within a canopy width of 30–60 cm and plant height of 60–100 cm, while accommodating a payload capacity of 200 g. The final prototype consisted of 9 major links with individual link lengths ranging from 20 mm (wheel) to 200 mm (shoulder), resulting in an overall reach of approximately 700 mm. The lightweight design was achieved through FDM-based 3D printing using PLA+ with link weights between 0.05–0.50 kg. The end-effector combined flexible TPU gripper fingers with a stainless-steel scissor for peduncle cutting.
2. Finite Element Analysis (FEA) was conducted independently on each robotic link under direction-specific operational loads using SolidWorks Simulation (Premium 2022, Dassault Systèmes, France). The highest von Mises stress was observed in Link 2 at 5.644×10^5 Pa, corresponding to its role as the main load-bearing shoulder segment. The lowest stress occurred in Link 1_wheel at 8.529×10^3 Pa. Maximum displacement was noted in Link 5 at 2.53×10^{-2} mm, and minimum in Link 1_wheel at 3.460×10^{-5} mm. The minimum factor of safety (FoS) was 88.58, again in Link 2, well above the critical threshold relative to PLA+ yield strength (50 MPa), confirming mechanical robustness under worst-case harvesting loads.
3. The ROS 2-based simulation environment using RViz2 and MoveIt2 validated the robot's reachability, pose tracking, and motion feasibility. The URDF model accurately replicated forward kinematics with a mean end-effector position error of 2.3 mm across 20 pose samples. Joint angle profiles demonstrated sequential motion from θ_1 to θ_6 over a 6-second harvesting cycle, with θ_1 rotating 45° and θ_6 activating at 5 s for gripping. The polar reachability envelope confirmed a circular planar workspace with a maximum radial reach of 0.70 m. A 3D workspace comparison showed complete overlap with the capsicum canopy volume (0.40 m radius), ensuring full accessibility of fruit locations with a margin for path optimization.

The study thus successfully delivers a fully integrated design, structural validation, and kinematic simulation framework for a 6-DOF robotic arm tailored to high-precision, non-destructive capsicum harvesting within greenhouse environments. The proposed system demonstrates strong mechanical reliability, optimal reachability for the capsicum canopy space, and high kinematic accuracy using ROS 2-based simulations. While the robotic manipulator achieved biologically relevant pose accuracy and complete canopy coverage in simulation, current validation was limited to static targets and controlled conditions within a virtual environment. Future work will target real-time deployment under variable fruit occlusion and foliage complexity. Integration with mobile bases, low-power actuators, and trajectory optimization strategies will further enhance the platform's adaptability for large-scale horticultural operations. Moreover, incorporating adaptive motion planning under multi-object occlusion is

expected to improve system generalization, decision-making under uncertainty, and the real-world applicability of the proposed harvesting framework.

Funding: This research was supported by the Indian Institute of Technology, Kharagpur, West Bengal (Grant number: PMRF 2402325).

Institutional Review Board Statement: Not applicable.

Transparency: The authors state that the manuscript is honest, truthful, and transparent, that no key aspects of the investigation have been omitted, and that any differences from the study as planned have been clarified. This study followed all writing ethics.

Competing Interests: The authors declare that they have no competing interests.

Authors' Contributions: Both authors contributed equally to the conception and design of the study. Both authors have read and agreed to the published version of the manuscript.

Disclosure of AI Use: During the preparation of this work, I utilized ChatGPT (OpenAI, GPT-4o model, accessed via <https://chat.openai.com>) solely for enhancing the language clarity of certain sections. The tool was not used for content generation, data analysis, or drawing scientific conclusions. After using this service, I thoroughly reviewed and edited the content as necessary, and I take full responsibility for the final content of the published article.

REFERENCES

- [1] A. Paul, R. Machavaram, Ambuj, D. Kumar, and H. Nagar, "Smart solutions for capsicum Harvesting: Unleashing the power of YOLO for detection, segmentation, growth stage classification, counting, and real-time mobile identification," *Computers and Electronics in Agriculture*, vol. 219, p. 108832, 2024. <https://doi.org/10.1016/j.compag.2024.108832>
- [2] A. Paul and R. Machavaram, "Greenhouse capsicum detection in thermal imaging: A comparative analysis of a single-shot and a novel zero-shot detector," *Next Research*, vol. 1, no. 2, p. 100076, 2024. <https://doi.org/10.1016/j.nexres.2024.100076>
- [3] A. Kaleem, S. Hussain, M. Aqib, M. J. M. Cheema, S. R. Saleem, and U. Farooq, "Development challenges of fruit-harvesting robotic arms: A critical review," *AgriEngineering*, vol. 5, no. 4, pp. 2216-2237, 2023. <https://doi.org/10.3390/agriengineering5040136>
- [4] M. Xie, *Fundamentals of robotics: linking perception to action*. Singapore: World Scientific Publishing Company, 2003.
- [5] Y. Fan, X. Lv, J. Lin, J. Ma, G. Zhang, and L. Zhang, "Autonomous operation method of multi-DOF robotic arm based on binocular vision," *Applied Sciences*, vol. 9, no. 24, p. 5294, 2019. <https://doi.org/10.3390/app9245294>
- [6] R. Barth *et al.*, "Using ROS for agricultural robotics-design considerations and experiences," in *Proceedings of the Second International Conference on Robotics and Associated High-Technologies and Equipment for Agriculture and Forestry*, 2014, pp. 509-518.
- [7] K. Rahul, H. Raheman, and V. Paradkar, "Design of a 4 DOF parallel robot arm and the firmware implementation on embedded system to transplant pot seedlings," *Artificial Intelligence in Agriculture*, vol. 4, pp. 172-183, 2020. <https://doi.org/10.1016/j.aiia.2020.09.003>
- [8] L. Van Herck, P. Kurtser, L. Wittemans, and Y. Edan, "Crop design for improved robotic harvesting: A case study of sweet pepper harvesting," *Biosystems Engineering*, vol. 192, pp. 294-308, 2020. <https://doi.org/10.1016/j.biosystemseng.2020.01.021>
- [9] Z. Liming, H. Yulong, X. Shanjun, Z. Tong, G. Junlong, and W. Mingrui, "Mechanical design and finite element analysis of live working robot for 10kV distribution power systems," *Procedia Computer Science*, vol. 183, pp. 331-336, 2021. <https://doi.org/10.1016/j.procs.2021.02.067>
- [10] J. Huanca, J. Zamora, J. Cornejo, and R. Palomares, "Mechatronic design and kinematic analysis of 8 DOF serial robot manipulator to perform electrostatic spray painting process on electrical panels," presented at the 2022 IEEE Engineering International Research Conference (EIRCON), IEEE, 2022.
- [11] C. Paredes, R. Palomares, J. Alva, and J. Cornejo, "Mechatronics design and robotic simulation of serial manipulators to perform automation tasks in the avocado industry," *International Journal of Advanced Computer Science and Applications*, vol. 14, no. 8, pp. 509-517, 2023. <https://doi.org/10.14569/IJACSA.2023.0140856>

- [12] M. Salazar and P. Portero, "CAD design and modeling of a robotic Arm for automated harvesting," in *Proceedings of the International Conference on Robotics and Automation, IEEE*, 2024, pp. 123–130.
- [13] H. Li and Y. Li, "Finite element analysis and structural optimization design of multifunctional robotic arm for garbage truck," *Frontiers in Mechanical Engineering*, vol. 11, p. 1543967, 2025. <https://doi.org/10.3389/fmech.2025.1543967>
- [14] J. K. Kuruvilla, A. Seth, J. Duttagupta, S. Sharma, and A. Jaiswal, *Structural design and analysis of 6-DOF cylindrical robotic manipulators for automated agriculture. In Precision Agriculture for Sustainability*. USA: Apple Academic Press, 2024.
- [15] D. Zhang, Y. Xu, Z. Hou, J. Yao, and Y. Zhao, "Optimal design and kinematics analysis of 5-dof hybrid serial-parallel manipulator," *Transactions of the Chinese Society of Agricultural Engineering*, vol. 32, no. 24, pp. 69–76, 2016.
- [16] A. Amir, A. Verma, A. Goswami, A. Kabra, S. Nakhye, and S. Chaudhary, "Design and analysis of strawberry-picking industrial Robotic Arm," presented at the 2022 IEEE Bombay Section Signature Conference (IBSSC), IEEE, 2022.
- [17] D. Bauer, C. Bauer, A. Lakshmipathy, and N. Pollard, *Fully printable low-cost dexterous soft robotic manipulators for agriculture. In AI for Agriculture and Food Systems*. United Kingdom: Springer Nature, 2022.
- [18] F. Wang and Y. Fan, "Structural design and analysis of a picking robot arm using parallel grippers," *Advances in Mechanical Engineering*, vol. 16, no. 12, p. 16878132241304610, 2024. <https://doi.org/10.1177/16878132241304610>
- [19] Z. Wang, L. Gong, Q. Chen, Y. Li, C. Liu, and Y. Huang, "Rapid developing the simulation and control systems for a multifunctional autonomous agricultural robot with ROS," in *Intelligent Robotics and Applications: 9th International Conference, ICIRA 2016, Tokyo, Japan, August 22-24, 2016, Proceedings, Part I 9, Springer International Publishing*, 2016, pp. 26–39.
- [20] D. Sepúlveda, R. Fernández, E. Navas, P. González-de-Santos, and M. Armada, "ROS framework for perception and dual-arm manipulation in unstructured environments," presented at the Robot 2019: Fourth Iberian Robotics Conference: Advances in Robotics, Springer International Publishing, 2019.
- [21] W. Chen and F. Liu, "Design of a grasping robot control system using kinematics model," *Journal of Physics: Conference Series*, vol. 2083, no. 2, p. 022031, 2021. <https://doi.org/10.1088/1742-6596/2083/2/022031>
- [22] Dassault Systèmes, *Solidworks (Version 2022)*. France: Dassault Systèmes, 2023.
- [23] Open Robotics, *ROS 2 humble Hawksbill (Version 2)*. United States: Open Robotics, 2022.

Views and opinions expressed in this article are the views and opinions of the author(s). Current Research in Agricultural Sciences shall not be responsible or answerable for any loss, damage or liability etc. caused in relation to/arising out of the use of the content.